Bioactive Materials 37 (2024) 94–105

Contents lists available at ScienceDirect

Bioactive Materials

journal homepage: www.keaipublishing.com/en/journals/bioactive-materials

Aiming at early-stage vulnerable plaques: A nanoplatform with dual-mode imaging and lipid-inflammation integrated regulation for atherosclerotic theranostics

Yao Wang [a,b], Zhebin Chen [a,b], Qiongjun Zhu [a,b], Zhezhe Chen [a,b], Guosheng Fu [a,b,**], Boxuan Ma [a,b,*], Wenbin Zhang [a,b,***]

[a] Department of Cardiology, Sir Run Run Shaw Hospital, School of Medicine, Zhejiang University, Hangzhou, China
[b] Key Laboratory of Cardiovascular Intervention and Regenerative Medicine of Zhejiang Province, Hangzhou, China

ARTICLE INFO

Keywords:
Atherosclerosis
Theranostics
Nanoplatform
Dual-mode imaging
Lipid-inflammation integrated regulation

ABSTRACT

The vulnerable plaques in atherosclerosis can cause severe outcome with great danger of acute cardiovascular events. Thus, timely diagnosis and treatment of vulnerable plaques in early stage can effectively benefit the clinical management of atherosclerosis. In this work, a targeting theranostic strategy on early-stage vulnerable plaques in atherosclerosis is realized by a LAID nanoplatform with X-CT and fluorescent dual-mode imaging and lipid-inflammation integrated regulation abilities. The iodinated contrast agents (ICA), phenylboronic acid modified astaxanthin and oxidized-dextran (oxDEX) jointly construct the nanoparticles loaded with the lipid-specific probe LFP. LAID indicates an active targeting to plaques along with the dual-responsive disassembly in oxidative stress and acidic microenvironment of atherosclerosis. The X-CT signals of ICA execute the location of early-stage plaques, while the LFP combines with lipid cores and realizes the recognition of vulnerable plaques. Meanwhile, the treatment based on astaxanthin is performed for restraining the progression of plaques. Transcriptome sequencing suggests that LAID can inhibit the lipid uptake and block NF-κB pathway, which synergistically demonstrates a lipid-inflammation integrated regulation to suppression the plaques growing. The *in vivo* investigations suggest that LAID delivers a favorable theranostics to the early-stage vulnerable plaques, which provides an impressive prospect for reducing the adverse prognosis of atherosclerosis.

1. Introduction

Atherosclerosis serves as the primary etiological factor for the majority of myocardial infarctions and a significant number of strokes, as well as the development of debilitating peripheral artery disease [1,2]. The gradual advancement of atherosclerosis often results in an extended asymptomatic phase lasting several decades, with symptomatic manifestations typically arising from diminished blood flow caused by luminal stenosis or thrombotic occlusion [3,4]. Initiated by the accumulation of low-density lipoprotein (LDL) particles and inflammatory cells within the intima layer of the artery wall, foam cells and plaques are formed at the early stage of atherosclerosis. In further with the proliferation and death of smooth muscle cells (SMCs) and macrophages, the necrotic cores and fibrous caps in the plaques progress with accelerated threat to life [5,6]. Within different development degrees of the plaques, unstable plaques with a thin fibrous cap, minimum lumen area and characteristic lipid arcs in clinics, are a form of atherosclerotic lesions that characterized with growing lipid core and exhibit a proclivity for rupture, thereby inducing thrombosis and precipitating acute cardiovascular events, resulting in acute coronary syndrome or stroke [7,8]. Thus, the timely identification of early-stage vulnerable plaques acts an important role in reducing the poor prognosis of atherosclerosis.

The atherosclerotic plaques are diagnosed in clinics by means of direct visualization methods such as intravascular ultrasound (IVUS), magnetic resonance imaging (MRI) and optical coherence tomography

Peer review under responsibility of KeAi Communications Co., Ltd.
* Corresponding author. Department of Cardiology, Sir Run Run Shaw Hospital, School of Medicine, Zhejiang University, Hangzhou, China.
** Corresponding author. Department of Cardiology, Sir Run Run Shaw Hospital, School of Medicine, Zhejiang University, Hangzhou, China.
*** Corresponding author. Department of Cardiology, Sir Run Run Shaw Hospital, School of Medicine, Zhejiang University, Hangzhou, China.
E-mail addresses: fugs@zju.edu.cn (G. Fu), boxuanma@zju.edu.cn (B. Ma), 3313011@zju.edu.cn (W. Zhang).

https://doi.org/10.1016/j.bioactmat.2024.03.019
Received 8 October 2023; Received in revised form 19 February 2024; Accepted 13 March 2024

(OCT) [9,10], while the plaque activity and vulnerability can also be measured by the non-direct visualization methods such as positron emission tomography (PET) and invasive coronary angiography [11,12]. Nevertheless, the current diagnostic methods in clinics still suffer from several drawbacks including contrast agent toxicity, low spatial resolution, long acquisition time and vascular selectivity [13,14]. Moreover, the lack of obvious symptom of early-stage plaques without blood-limiting lesions also hinders the timely diagnosis, and the accurate diagnosis on vulnerable plaques still requires feasible means to realize [15,16]. In recent years, the various targeting probes have been developed to recognize the pathological component of plaques instead of hemodynamic detection, which provides a potential practicality for diagnosis of early-stage lesions in atherosclerosis [17,18]. Besides, within the fast-progressing research on diversiform imaging technique, fluorescent imaging has been proven to be optimal for high-resolution observation of biological microstructures, where a series of molecules with lipid-specific imaging capabilities are developed, offering several possible candidate molecules for the identification of lipid cores in atherosclerosis [19–21].

Lipid metabolism and inflammation are tightly implicated in the overall advancement of atherosclerosis. Endothelial dysfunctions by inflammation are considered as the initial step to atherosclerosis. Concurrently, LDL can be modified and converted into oxidized LDL (oxLDL), which is subsequently engulfed by macrophages and SMCs *via* scavenger receptors (SRs), oxLDL receptors, and Toll-like receptor 4 (TLR4) [22–24]. To prevent this initial step, lipid-lowering agents, such as statins or PCSK9 inhibitors have been utilized in primary prevention of early-stage atherosclerosis [25,26]. What's more, the inflammation mediators such as nuclear factor-kappa B (NF-κB), matrix metalloproteinase (MMP) and M1 macrophages, are present in early phases of atherosclerotic lesions which can trigger the vicious circle to deteriorate the plaques [27,28]. Several clinical trials have shown that anti-inflammatory therapy with canakinumab and colchicine that targets the IL-1β innate immunity pathway achieves a significant reduction-rate of recurrent cardiovascular events compared to independent lipid-lowering therapy and placebo [29,30]. Although atherosclerosis can be detected with relatively less complicated symptoms in its early stage, which can be effectively controlled with pharmacotherapy, the lack of timely diagnosis can be the critical challenge for clinical practice.

In order to practically control the progression of atherosclerosis, the nano-sized carriers offer a rational strategy towards early-stage atherosclerosis, which are constructed combining accurate diagnosis and efficient treatment abilities [31,32]. As nano-carriers developed in the past decades, the expanding applications based on nanoplatform have entered the clinical market for targeting diagnosis and drug delivery in atherosclerosis as well as the other diseases [33–36]. According to the pathogenesis of atherosclerosis, the broken endothelium at the plaques naturally provides a pathway for the accumulation of nanosized particles [37,38]. On the other hand, with the targeted design to the pathological features, the nanoplatform can be customized with active targeting to the atherosclerotic plaques with minimum recognition and clearance by the human immune system [39–41]. With the active inflammatory reaction in the plaques, the oxidative stress in macrophages and foam cells generates excess reactive oxygen species (ROS), while the vigorous anaerobic metabolism can produce the acidic environment with a pH of about 6.5 [42,43]. As a result, the stimuli-responsive nano-structure to the specific microenvironment in atherosclerotic lesions can assist to the efficient delivery of the cargos for diagnosis and treatment [44,45]. Jointly, the well-designed nanoplatform reduced side effect caused by non-specific distribution of the loadings, while intensifying the accumulation at the target site at the same time, thus providing a meaningful approach for the promoted theranostic outcome.

Herein, a targeting nanoplatform LAID is designed and constructed for the dual-mode diagnosis and lipid-inflammation integrated regulation of early-stage vulnerable plaques in atherosclerosis. The dual-mode diagnosis is achieved by fluorescent imaging and X-CT imaging based on lipid-specific probe LFP and iodinated contrast agents (ICA), while the astaxanthin is chosen as the therapeutic ingredients for the treatment of atherosclerosis. As the hydrophobic core, astaxanthin is grafted with phenylboronic acid (AST), which is bridged with ICA *via* the borate bonds. Besides, the amino groups on ICA can further construct the imine linkage with the aldehyde groups on oxidized dextran (oxDEX), which is introduced for the active targeting to the plaques through CD44 pathway [46–51]. With the self-assembly of AST, ICA and oxDEX, the core-shell structured nanoparticle LAID is prepared, where the LFP probe is loaded into the AST hydrophobic core (Scheme 1A).

On account of the oxDEX surface, the LAID nanoparticles can maintain a stable transformation in blood after injection, which can specifically recognize the overexpressed CD44 on activated endothelium and foam cells in plaques. Thus, along with the passive enrichment provided by the nano-structure, LAID can efficiently target to the early-stage atherosclerotic lesions with the minimized loss in blood. When accumulated in the plaques, the local overexpressed ROS and acidic environment can trigger the breakage of borate bonds and imine linkages of LAID, leading to the disassembly of nanoparticles and the release of ICA, LFP and astaxanthin. Under the detection of X-CT, ICA reveals a significant positive signal, which can realize the *in vivo* location of early-stage plaques. In further, the LFP probe can be combined with the lipid core in vulnerable plaques for a specific fluorescent emission at about 530 nm, which indicates the recognition of vulnerable plaques in their early-stage. On the other side, astaxanthin is utilized to restrain the deterioration of atherosclerosis, which has been reported with cardioprotective effects in various animal models and human studies through modulating lipid metabolism, reducing inflammation and preventing oxidative stress [52–55]. Based on this, the therapeutic mechanism of LAID is studied using transcriptome sequencing, which suggest that a lipid-inflammation integrated regulation to atherosclerosis can be performed through the inhibition of lipid uptake and synergistical blockage of NF-κB pathway (Scheme 1B). Therefore, the accurate dual-mode diagnosis and the novel lipid-inflammation integrated regulation make this LAID nanoplatform a potential clinical solution for theranostics to the early-stage vulnerable plaques of atherosclerosis.

2. Results and discussion

2.1. Preparation and dual-responsiveness of LAID

To construct the LAID nanoparticles, the phenylboric acid modified astaxanthin (AST) was first synthesized *via* an esterification reaction. The chemical structure of AST was characterized by ^{1}H NMR spectra (Fig. S1). Subsequently, AST, ICA and oxDEX were used to prepare the LAID nanoparticles, where AST and ICA were linked *via* a borate bond, and an imine linkage was bridged between ICA and oxDEX (Scheme S2). During the construction procedure, the fluorescent probe LFP was loaded into the hydrophobic cores of AST. Thus, a core-shell structure of LAID nanoparticles was endowed with oxDEX as the hydrophilic s leading to the overexpression of ROS and an acidic microenvironment. hell and AST as the hydrophobic core, while ICA was utilized to crosslink the core-shell structure. The prepared nanoparticles was characterized by FT-IR, where the imine linkage and the boric acid ester were observed formed at the broad bands at 1645 and 1150 cm^{-1} (Fig. S2). The particle size of LAID was 112.1 nm with a PDI of 0.109 measured by dynamic light scattering (DLS), which maintained a regularly spherical morphology under TEM observation (Fig. 1A). And the size of controlled LAIP nanoparticle without crosslinking structure and targeting ability was also indicated by DLS and TEM shown in Fig. S3. The crosslinked nanostructure and a hydrophilic oxDEX surface could provide a satisfied stability of LAID during transporting in the blood circulation, which was confirmed *in vitro* by measuring the size under long-term incubation in PBS and 10% FBS solutions (Fig. S4) as compared with the uncrosslinked LAIP. Furthermore, the stability of LAID after dilution was also

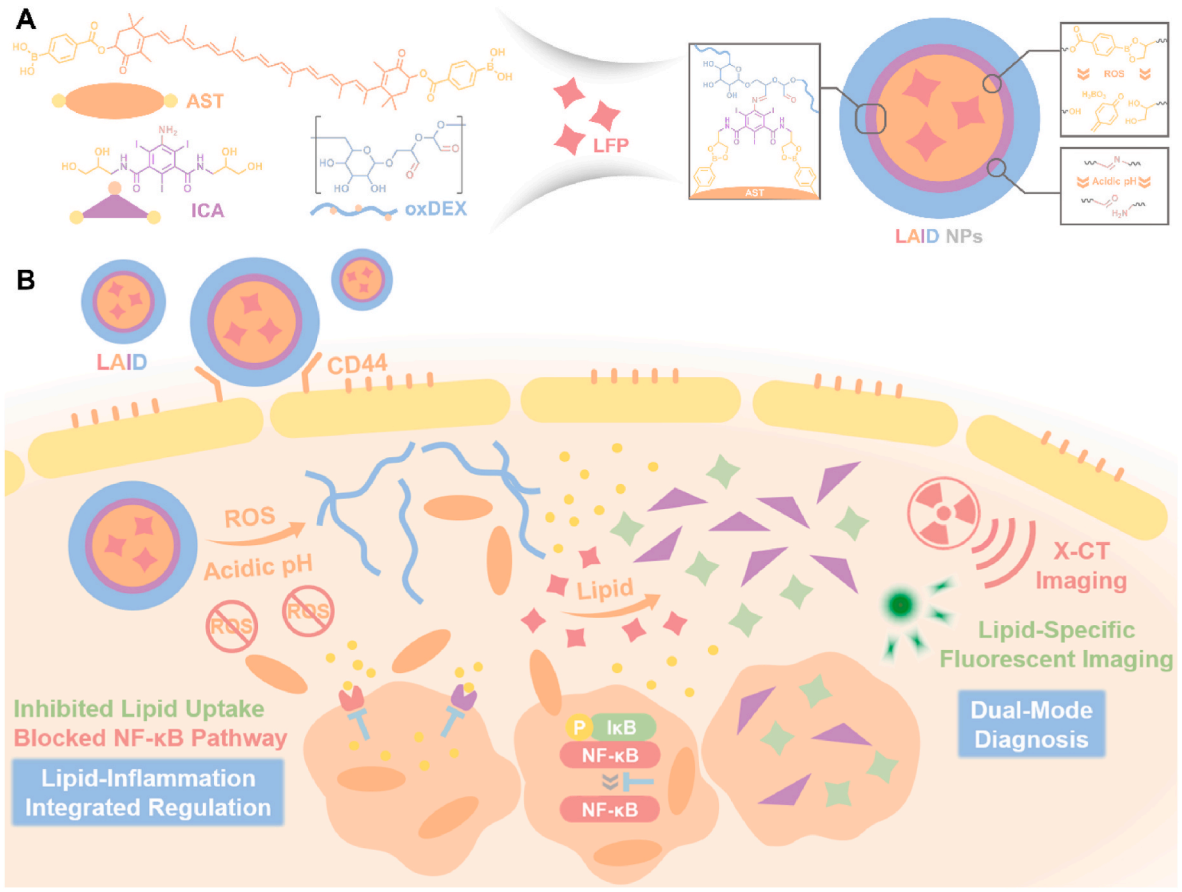

Scheme 1. Illustration of LAID nanoplatform for the theranostics of early-stage vulnerable plaques in atherosclerosis. A) The construction of LAID nanoplatform. B) The theranostic procedure including the active targeting, the ROS and acid dual-triggered disassembly, the X-CT based plaque location, the lipid recognition with fluorescent imaging, and the lipid-inflammation integrated regulation *via* inhibited lipid uptake and blocked NF-κB pathway.

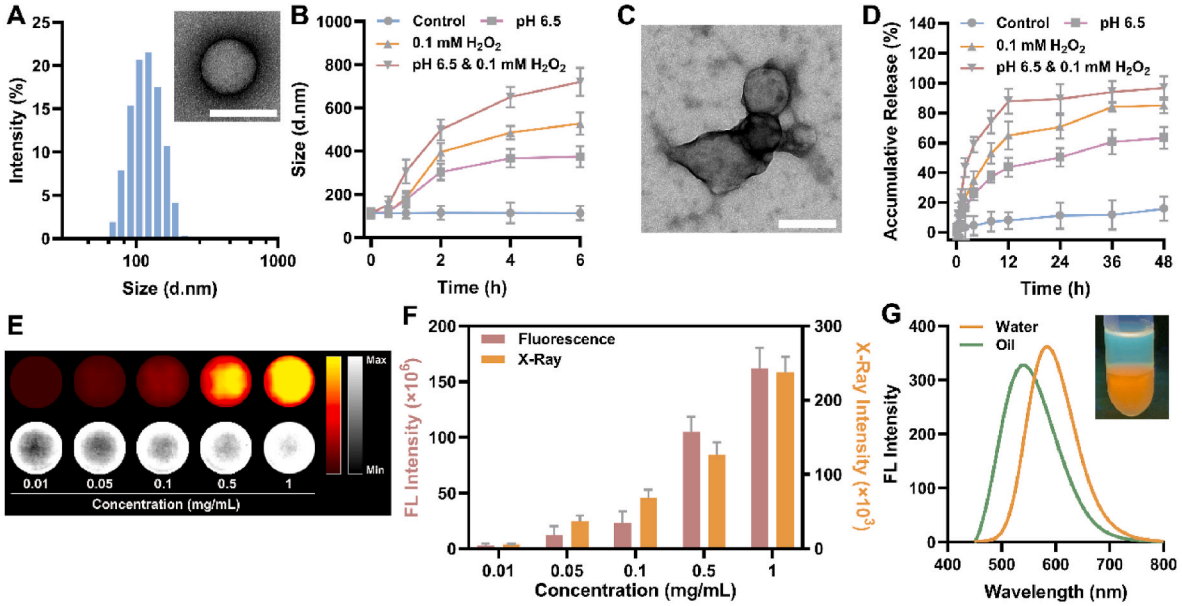

Fig. 1. Preparation and characterization of LAID. A) Particle size of LAID nanoparticles measured by DLS as well as the TEM image. The scale bar was 100 nm. B) Variation of particle size when LAID cultured in different conditions. C) TEM image of LAID after incubation in 0.1 mM H_2O_2 solution at pH 6.5 for 4 h. The scale bar was 100 nm. D) Astaxanthin release behavior of LAID under different stimulations. E) Fluorescent and X-ray images and F) quantitative intensity of LAID with various concentration. G) Fluorescent spectrum and photographs of LAID in water and oil solutions after treated with 0.1 mM H_2O_2 at pH 6.5. Data in (B, D, F) were expressed as mean ± s.d. (n = 3).

evaluated (Fig. S5). The uncrosslinked LAIP was observed interrupted at a lower concentration with the increasing particle size, while LAID remained the stability owing to its crosslinked structure, thus providing a stable transformation in blood stream.

The progressive inflammation was identified as the main pathological feature in atherosclerotic lesions, especially in early vulnerable plaque, which showed an active infiltration of inflammatory cells such as monocytes and macrophages. As a result, the local oxidative stress as well as hypoxia and lactic acid production were discovered in the plaques, leading to the overexpression of ROS and an acidic microenvironment [56,57]. Aiming to this pathological microenvironment, LAID was designed with dual-responsiveness against acidic pH and overexpressed ROS. The acidic pH at 6.5 could cause the breakage of imine linkage between ICA and oxDEX, and the ROS condition could further trigger the disassembly of nanoparticles by breaking the borate bond between AST and ICA. The dual-responsiveness of LAID was first investigated by measuring the particle size to indicate the nano-structural disintegration. As shown in Fig. 1B, the particle size of LAID was detected significantly increased under the stimulation at pH 6.5, which was also confirmed by TEM (Fig. S6), while the ROS condition could accelerate the disassembly of nanoparticles. With the existence of ROS at pH 6.5, the LAID indicated the most drastic increase of particle size, which was also confirmed by TEM shown in Fig. 1C, where distinct aggregates were observed under ROS and acidic environment. Furthermore, the delivery of astaxanthin was also measured under different stimulations and shown in Fig. 1D. While the LAID nanoparticles exhibited a well stability within 48 h with few leakages of astaxanthin (less than 15%), the acidic pH could cause the release of astaxanthin to some extent with about 60% released in 48 h. Moreover, the ROS condition demonstrated a promoted astaxanthin release with over 80% released in 48 h. In together, the most efficient astaxanthin delivery was observed with the co-stimulation of ROS and acid, where over 95% of the cargos were released after 48 h. On the other side, the ROS responsive behavior of AST to astaxanthin was also confirmed by FT-IR (Fig. S7), where the broad band at 1670 and 1630 cm^{-1} belonging to the benzene ring and ester bond disappeared. In further, the influence of crosslinked structure on drug release of LAID was also checked as compared with the uncrosslinked LAIP (Fig. S8). Even though the drug release of LAID was observed slower respectively in single stimulations of acidic pH or ROS, due to the rapid responsiveness, the drug release behavior under both acidic and ROS condition declared no significant differences with or without crosslinking. Thus, after accumulating at the atherosclerotic lesions, an efficient delivery of diagnostic ICA and LFP probe as well as the therapeutic astaxanthin was expected to achieve due to this dual-responsiveness on the ROS and acidic microenvironment.

2.2. In vitro dual-mode imaging of LAID

In order to locate the plaques along with identifying the lipid composition of the plaques, LAID was endowed with dual-mode imaging ability including X-CT and fluorescent imaging. The *in vitro* imaging ability was studied respectively and shown in Fig. 1E and **F**. The intensities of both fluorescence and X-ray were discovered increased with the raising concentration of nanoparticles. On the other hand, the lipid specific imaging offered by LFP was also characterized in LAID. It was observed that the acidic pH could not solely trigger the fluorescent differentiation of LAID in oil/water solution (Fig. S9). On the other side, after the disassembly of LAID under ROS and acidic condition at pH 6.5, the LFP probe was released and specifically combined with the oil phase or lipids, which further revealed a special green fluorescence under the excitation at 450 nm (Fig. 1G). The fluorescent spectrum also proved that a lipid-specific emission wavelength at 530 nm was measured, while the water solution of LAID showed an emission wavelength at 600 nm, which demonstrated an accurate recognition on lipid core of vulnerable plaque owing to this lipid-specific fluorescent imaging.

2.3. In vitro theranostics on foam cells

Owing to the selective interaction between oxDEX and CD44 on the activated endothelium and foam cells, LAID was expected to accumulated at atherosclerotic lesions through active targeting. Thus, the local theranostics of LAID towards lipid-deposited foam cells were studied *in vitro*. Above all, the cytocompatibility of LAID was confirmed on RAW 264.7 cells and endothelial cells (Fig. S10). Then the internalization of LAID in macrophages was further traced by fluorescent and X-ray imaging shown in Fig. 2A and B. The strengthening fluorescent and X-ray intensity detected in cells indicated the gradually accumulation of LAID nanoparticles within 6 h, which was laying for the further plaque location as well as lipid recognition. The lipid specific imaging of LFP probe on foam cells was first confirmed (Fig. S11). The lipid droplets in foam cells could be accurately recognized by LFP, which was co-located with the signal belonging to a commercially available lipid probes Lipid Blue. Subsequently, the lipid-specific fluorescent imaging of LAID on foam cells was investigated with RAW 264.7 cells as a control. As shown in Fig. 2C and **D**, the LAID only showed a stronger red fluorescent signal in RAW 264.7 cells over time. Nevertheless, with the deposited lipid, the foam cells exhibited a gradually enhanced green fluorescence after internalizing LAID with LFP probe loaded, while the red fluorescent signal was observed weakened after 4 h. Moreover, the lipid specific imaging was also studied by flow cytometry (Fig. 2E). While the RAW 264.7 cells revealed a time-dependent internalization of LAID with increasing fluorescent intensity at 580–630 nm (Fig. 2F), the specific imaging on foam cells showed a clear fluorescent differentiation into red and green channels. During the first 2 h of internalization by foam cells, LAID could maintain its nano-structure with a major emission of red fluorescence (Fig. 2G). However, with the time extension, the nanoparticles were interrupted and LFP was released exhibiting the lipid-specific green fluorescence (Fig. 2H). As a result, a weak red fluorescence and a strong green fluorescence could be observed after 4 h, suggesting a splendid dual-responsive lipid-specific cellular imaging by LAID (Fig. 2I).

Atherosclerosis was characterized by progressive inflammation and lipid deposition, which was primarily affected by macrophages and foam cells. Thus, according to the previous studies on antioxidant of astaxanthin [54,58], the treatment offered by LAID was expected to achieve an inhibition on foam cells formation. On account of the strong association of intracellular ROS with the inflammatory reactions, the resistance of LAID against oxidative stress was first investigated in stimulated macrophages. As shown in Fig. 2J and **K**, the green fluorescent signal of ROS probe DCFH-DA could be obviously found in the saline treated cells after stimulated by lipopolysaccharide (LPS). On the contrary, LAID delivered a concentration-dependent antioxidation, where only faintest ROS signals could be observed when the LAID concentration reached 100 μg mL^{-1}. Furthermore, the inhibition on foam cell formation provided by LAID was also studied to evaluate its potential on atherosclerosis therapy (Fig. 2L and **M**). In accordance with the antioxidation results, LAID exhibited a significant prevention of foam cell formation at the concentration higher than 50 μg mL^{-1}, and the 100 μg mL^{-1} of LAID revealed the best inhibition on foam cell formation. As the result, the antioxidation and suppression of foam cell formation made LAID beneficial for *in vivo* treatment of atherosclerosis.

2.4. In vivo dual-mode diagnosis on atherosclerosis

In clinical settings, the vulnerable plaques could cause great uncertainty and threat to patients' lives due to their uncontrollable growth and the risk of rupture at any moment. Hence, the timely recognition and distinction of vulnerable plaques at early stage was expected to effectively mitigate the adverse prognosis of atherosclerosis. The LAID nanoplatform was designed to perform a dual-mode diagnosis on early-stage vulnerable plaque through two steps. The early-stage plaques without obvious symptoms were first recognized with X-CT, which was

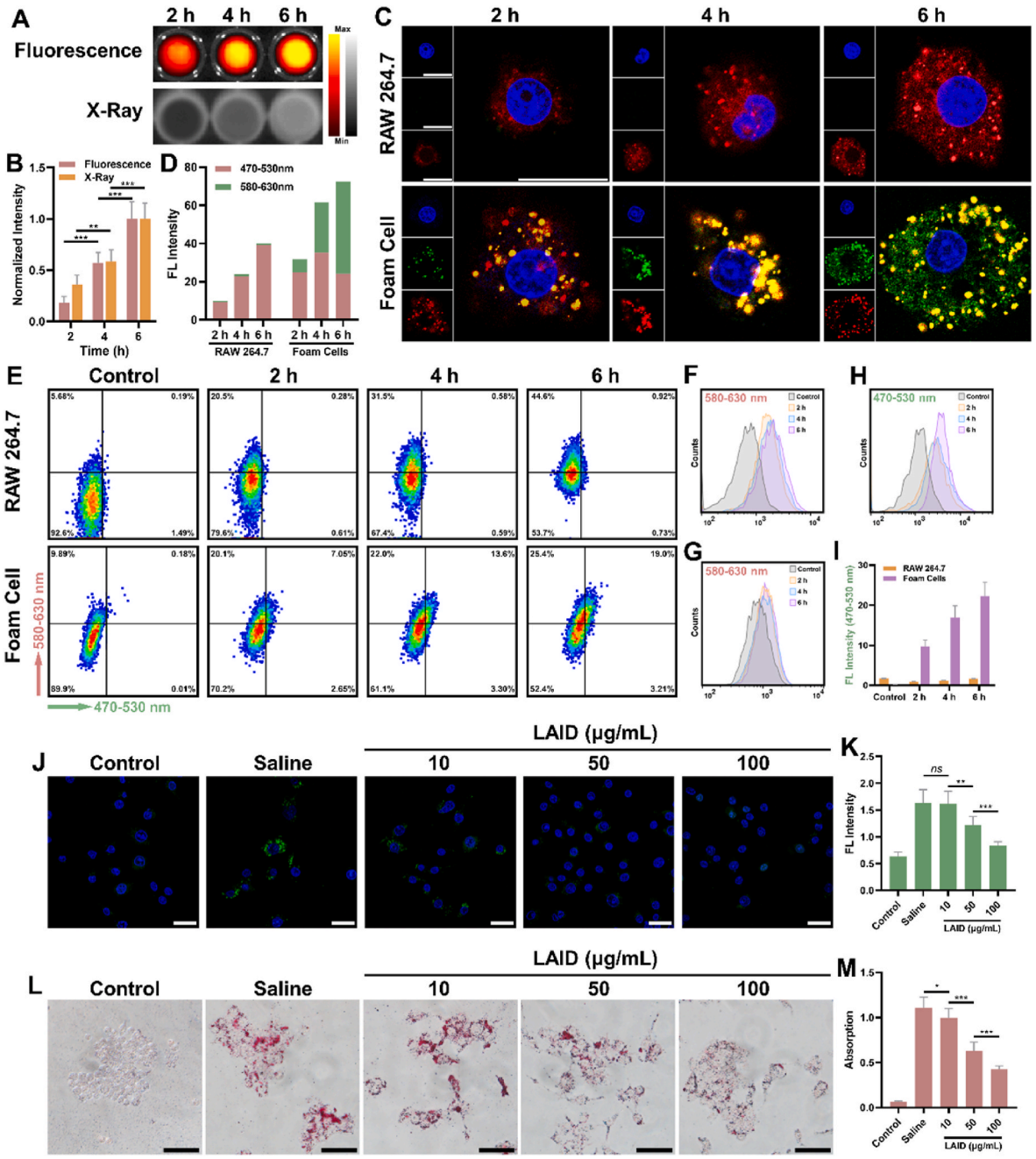

Fig. 2. *In vitro* theranostic ability of LAID. A) Fluorescent and X-ray images and B) normalized intensity of RAW 264.7 cells treated with LAID for different time. C) Confocal images and D) quantitative data of naïvely unpolarized RAW 264.7 and foam cells treated with LAID for various time. The red fluorescence indicated the LAID nanoparticles loaded with LFP. And the green fluorescence indicated the specific signal of LFP after combining with lipid droplet in foam cells. The scale bars were 20 μm. E) Flow cytometric results of cellular uptake and lipid-specific imaging of LAID in RAW 264.7 and foam cells. The red fluorescent channels of F) RAW 264.7 and G) foam cells, the H) green channel of foam cells were respectively analyzed along with the I) quantified result. J) Confocal images and K) quantitative result of ROS generation in stimulated macrophages treated with saline or LAID. The scale bars were 25 μm. L) Optical microscopy images and M) quantified data of ORO-stained foam cells with different stimulations. The scale bars were 100 μm. Data in (B, I, K, M) are expressed as mean ± s.d. (n = 3). $^{*}p < 0.05$, $^{**}p < 0.01$, $^{***}p < 0.001$; *ns*, no significance.

owing to the active targeting of LAID at atherosclerotic lesions offered by the oxDEX surface. Then the lipid-specific fluorescent imaging offered by LAID was utilized to distinguish the vulnerable plaque with lipid enrichment (Fig. 3A). The *in vivo* biosafety of LAID was first evaluated in ApoE$^{-/-}$ mice, where no visible acute toxicity was discovered in major organs (Fig. S12). Furthermore, the hemolysis test also indicated a satisfying biosafety of LAID in blood (Fig. S13). Afterwards, the active targeting ability of LAID mediated by oxDEX surface was compared with that of LAIP, which consisted of a non-targeted PEG surface (Fig. 3B and **C**). Depending on the passive enrichment provided by the broken endothelium of plaques, LAIP showed a considerable accumulation in aortas after 24 h from injection. On the other side, armed with oxDEX, LAID nanoparticles could achieve a CD44 mediated active targeting to the plaques with higher efficiency. Moreover, more LAIP was discovered in liver and kidney as compared with LAID, which also suggested more metabolism of LAIP rather than LAID (Fig. S14). The advantage of active targeting ability exhibited more obviously over. On the other hand, according to the pharmacokinetic result shown in

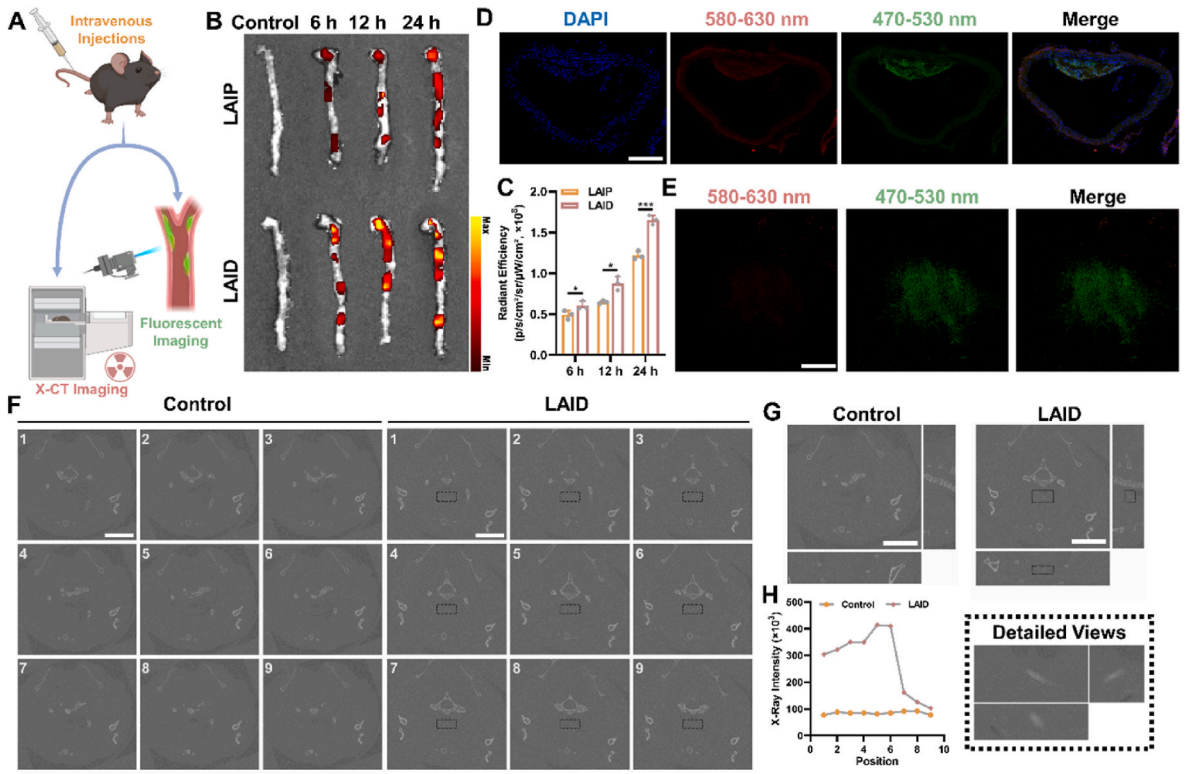

Fig. 3. *In vivo* dual-mode diagnosis of LAID on atherosclerosis. A) Scheme of LAID for fluorescent and X-CT imaging of atherosclerotic plaques. B) *Ex vivo* fluorescent images and C) quantified result of LAIP and LAID accumulated in aortas for different time. The fluorescent signals of emission wavelength at 550 nm and 600 nm were cumulatively recorded. D) CLSM images of the sections belonging to LAID treated aortas. The scale bar was 500 μm. E) Confocal images of aortic *en face* treated with LAID. The scale bar was 100 μm. F) Cross-section X-CT photos and G) typical cross-section with side-looking photos of atherosclerosis plaques. The signals of marked plaques were partial enlarged and the H) intensity was measured. The scale bars were 5 mm. Data in (C) is expressed as mean ± s.d. (n = 3). $^{*}p < 0.05$, $^{**}p < 0.01$, $^{***}p < 0.001$.

Fig. S15, the crosslinked structure and good stability also offered LAID a longer circulation time in blood. Thereby, the efficient targeting of LAID could deliver an accelerated diagnosis and a more effective treatment on atherosclerosis.

In order to distinguish the vulnerable plaque, the lipid-enrichment environment provided a marker for lipid specific fluorescent imaging. As shown in Fig. 3D and **E**, due to the dual-responsive degradation of LAID with the release of LFP probe, the lipid specific imaging could be carried out efficiently with strong green fluorescent signal observed in plaques both in sections and *en face* of aorta, which could identify the plaque as a vulnerable plaque. In further, the accuracy of diagnosis was confirmed by multiple staining with ORO, H&E and Masson to the recognized plaques (Fig. S16), which were identified as the vulnerable plaques with rich lipid and incomplete fiber hat. On the other hand, LAID was also endowed with the ability to recognize the early-stage plaques *via* the X-CT. According to the cross-sectional photos of thoracic aorta under X-CT, LAID could target the plaques and exhibit a distinct positive signal under X-ray as compared with the control group (Fig. 3F). The typical cross-sectional and side-looking photos of atherosclerosis plaques recognized by LAID was also shown in Fig. 3G, where the plaque could be observed clearly in detailed views. Besides, the X-ray intensity of plaques imaged by LAID in each cross-sectional photo was quantified (Fig. 3H). Under the targeting imaging offered by LAID, the plaques revealed a stronger X-ray intensity of over 4 folds than the control group, which provided a satisfactory strategy for the recognition of early-stage atherosclerotic plaques.

2.5. *In vivo* treatment on atherosclerosis

According to the active targeting ability provided by oxDEX surface as well as the dual-responsive ability under ROS and acidic microenvironment, LAID was expected to achieve the efficient accumulation at atherosclerotic lesions with the accurate delivery of the therapeutic astaxanthin, which could lead to a favorable outcome on atherosclerosis treatment. Following the protocol shown in Fig. 4A, the mice were sacrificed after 12 weeks and the plaque areas on aortas were first evaluated using ORO staining (Fig. 4B). As compared with saline treated group, LAIP showed a clear inhibition of plaque progression with less ORO positive area found on aortas, which indicated the beneficial effect of astaxanthin based therapy even without the active targeting ability of LAIP nanoparticles. At the same time, owing to the active targeting by its oxDEX surface, it was exciting to find that LAID delivered a better anti-atherosclerosis activity rather than LAIP, where the ORO-positive plaques were found obviously decreased (Fig. 4C). In order to further investigate the progression of plaques with various treatment, multiple staining on sections of aortic roots was also carried out and shown in Fig. 4D. In conformity to the result of ORO staining on aortic *en face*, the ORO sections of aortic roots also suggested that LAID demonstrated the best inhibition on plaque progression with the fewest lipid area discovered (Fig. 4E). In addition, according to the H&E staining on the sections, the saline treated group showed a severe necrotic core, while LAIP could reduce the area of necrosis. Besides, the group treated with LAID exhibited a relatively compact structure at the plaques, which also indicated that LAID delivered the optimal restraint on pathological necrosis of the cells in plaques (Fig. 4F). Moreover, the collagen in the plaques was also determined with Masson staining. As shown in Fig. 4G, due to the degradation of extracellular matrix in vulnerable plaques, the collagen was observed clearly weakened in the group treated with saline. In the contrast, both LAIP and LAID could protect the collagen structure to some extent, while LAID exhibited the better suppression on

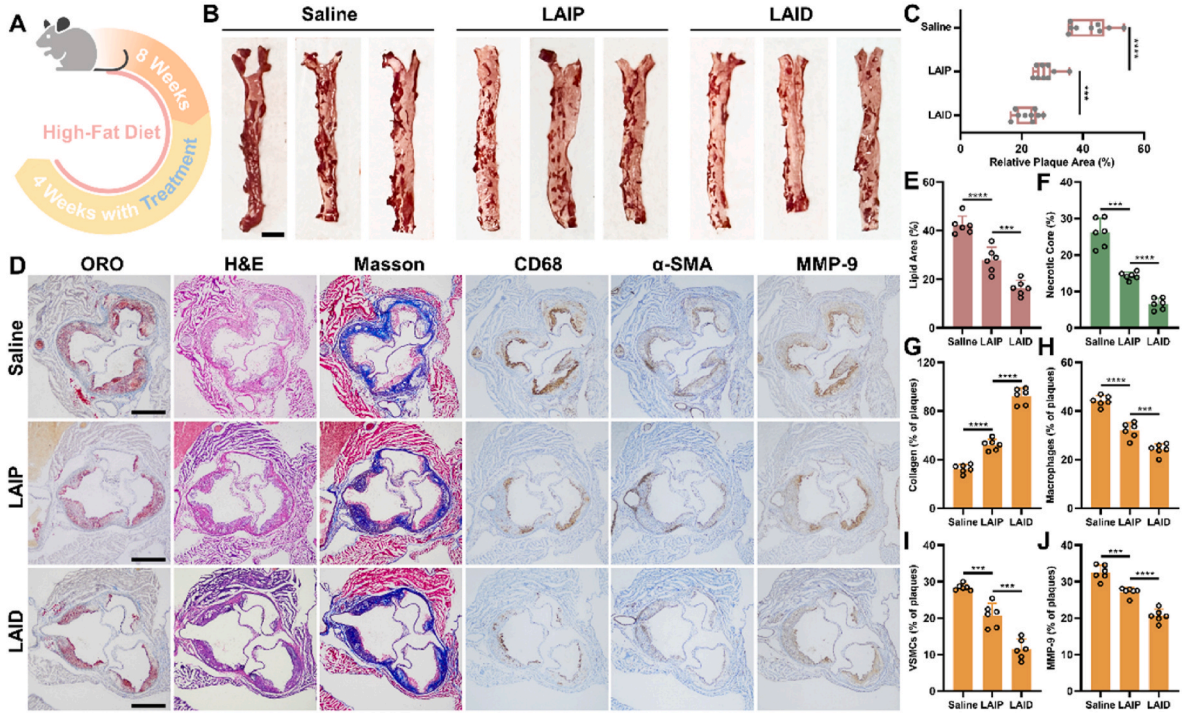

Fig. 4. *In vivo* treatment of LAID on atherosclerosis. A) Illustration of the treatment protocol on atherosclerosis. B) Photographs and C) relative area of plaques on the *en face* of aortas stained with ORO. The scale bar was 3 mm. D) Section of aortic roots stained with ORO, H&E, Masson's trichrome, CD68 antibody, α-SMA, and MMP-9 antibody after treated with Saline, LAIP and LAID. The scale bars were 500 μm. The quantitative results of E) lipid area, F) necrotic core, G) collagen generation, H) macrophages infiltration, I) VSMCs and J) MMP-9 expression were also calculated. Data in (C, E-J) are expressed as mean ± s.d. (n = 6). $^{*}p < 0.05$, $^{**}p < 0.01$, $^{***}p < 0.001$, $^{****}p < 0.0001$.

degradation of collagen. On the other side, the infiltration of macrophages and the migration of VSMCs could further accelerate the erosion of the plaques, which was evaluated with immunohistochemistry against CD68 and α-SMA antibodies (Fig. 4H and I). As compared with the control group, LAIP showed a reduced CD68 and α-SMA positive area, while LAID treated group was discovered with fewest macrophage infiltration as well as the minimum smooth muscle migration. Furthermore, the stabilization of the plaques was also studied by measuring the local MMP-9 expressing, where LAID indicated the greatest inhibition on MMP-9 expression (Fig. 4J). In together, owing to the active targeting and dual-responsive treatment based on astaxanthin, LAID delivered a better restrain on the progression of vulnerable plaques with fewer lipid, decreased necrosis and less macrophages infiltration, while simultaneously maintained a relative complete vascular structure with more collagen generation, inhibited smooth muscle migration and suppressed MMP-9. The exciting outcome of LAID revealed a potential of clinic practice of the treatment based on LAID nanoplatform, while the mechanism related to lipid metabolism and inflammatory reaction still required further development.

2.6. Mechanism studies of lipid-inflammation integrated regulation

According to the *in vitro* and *in vivo* demonstration, LAID exhibited a favorable anti-atherosclerosis activity, which was based on the therapeutic effect of astaxanthin. The previous studies had proved that astaxanthin was a strong antioxidant applicated in various diseases, while other works also indicated that astaxanthin could affected atherosclerosis through the lipid metabolism.[48,49] However, the mechanism of astaxanthin affecting inflammation and lipid metabolism was not clear enough. Thereby, the mechanism of LAID regulating atherosclerosis in this work was further investigated. Following the procedure shown in Fig. 5A, the whole transcriptome RNA sequencing of foam cells was carried out after treated with LAID. The genes of LAID treated group were highly diverse from the control group under multivariate analysis (principal component analysis, PCA), which was shown in Fig. 5B. 352 genes were observed down-regulated and 96 genes were up-regulated within the total 448 differential expressed genes (DEGs) (Fig. 5C and **D**). Among the top 10 significantly activated biological processes, the NF-κB signaling pathway and cholesterol metabolism pathway were focused, which was considered relating with the potential mechanism of LAID treatment on atherosclerosis (Fig. 5E). With in these two pathways, it was noted that five related genes (Cd36, Sort1, Syk, Blnk and Malt1) were discovered down-regulated, which could stimulate the suppression of lipid uptake as well as the inhibition of NF-κB mediated inflammatory reaction (Fig. 5F). As the key nodes of BCR-PKC–NF–κB pathway, the inhibition of Syk, Blnk and Malt1 genes could jointly restrain the activation of NF-κB pathway and the further inflammatory stress in foam cells. On the other hand, the down-regulated Cd36 and Sort1 genes, which led to the reduced expression of CD36 and Sortilin protein, could also inhibited the lipid uptake. Furthermore, the restrain of CD36 could also assist the control of PKC pathway [59,60], while the inhibition of Sortilin could retard the expression of IL-6 and TNF-α, resulting in the silence of TNF receptor (TNFR) and the restriction of NF-κB activating (Fig. 5G) [61,62]. Thus, LAID was supposed to execute the anti-atherosclerosis activity through this lipid-inflammation integrated regulation.

In order to verify the mechanism of this lipid-inflammation integrated regulation offered by LAID on atherosclerosis, the selected genes (Cd36, Sort1, Syk, Blnk and Malt1) were first characterized *in vitro* as well as the expression of CD36, Sortilin and NF-κB proteins. As the real-time PCR results shown in Fig. 6A-E, while the relative RNA expression of all five genes was up-regulated in the foam cells treated with saline, the LAID demonstrated an obvious callback of these genes, which was in accordance with the RNA-sequencing analysis. At the same time, the downstream CD36, Sortilin and NF-κB proteins were also quantified by Western Blot shown in Fig. 6F and **G**. As expected, the expression of

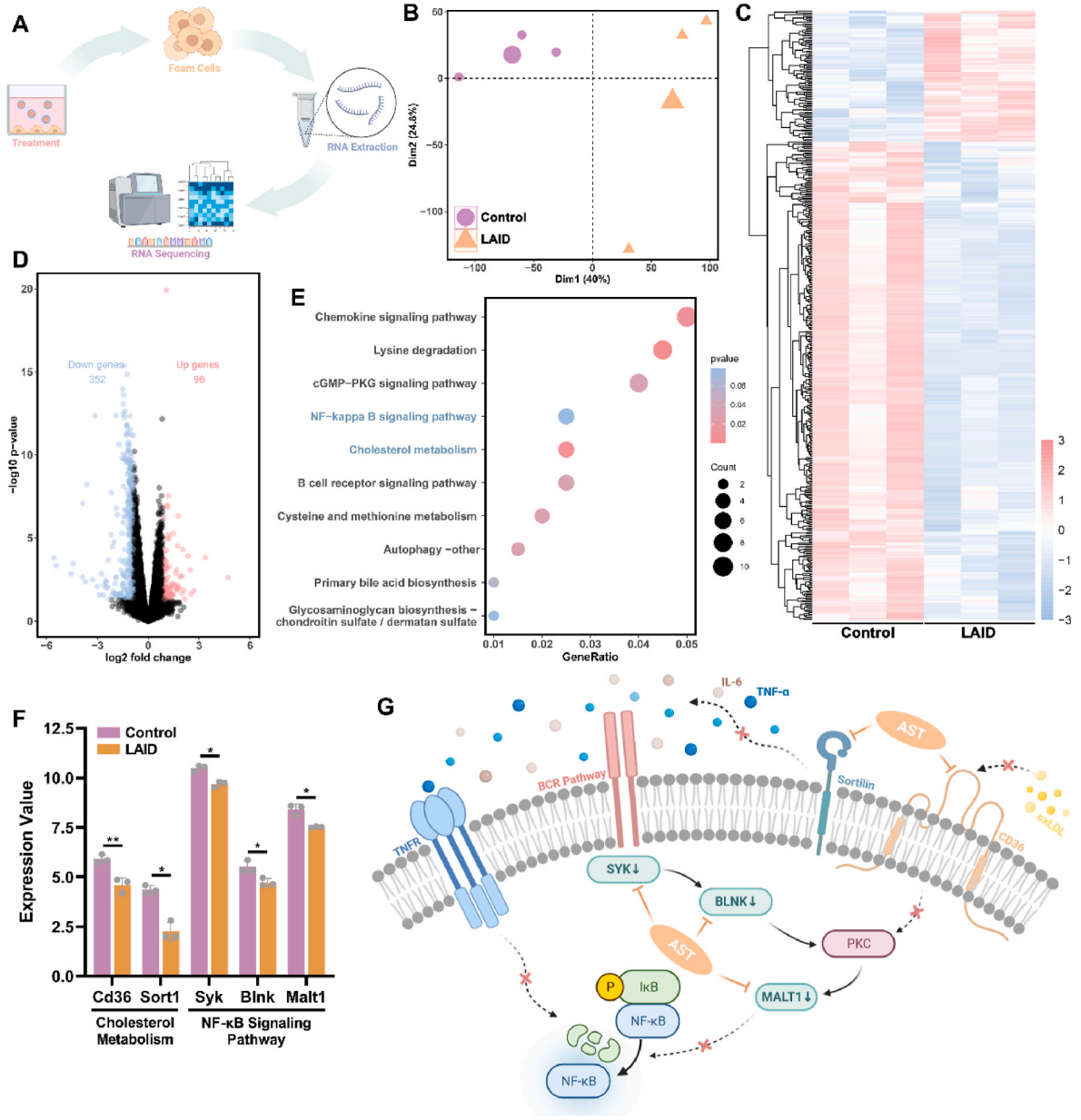

Fig. 5. RNA-sequence analysis of foam cells treated with LAID. A) Illustration on *in vitro* treatment on foam cells treated with LAID and RNA-sequence analysis procedure. B) PCA of genes in foam cells treated with LAID. C) Heatmap of differentially expressed genes in foam cells after treatment of LAID. D) The volcano plot of differentially expressed genes (DEGs). (p-value <0.01, |log2FC| > 0.78). E) Top 10 significantly activated biological processes analyzed based on DEGs. F) Typical differentially expressed genes in cholesterol metabolism and NF-κB signaling pathway. G) Illustrating the mechanism of lipid-inflammation integrated regulation of LAID on foam cells. Data in (F) are expressed as mean ± s.d. (n = 3). $^{*}p < 0.05$, $^{**}p < 0.01$.

CD36, Sortilin and NF-κB were all reduced after LAID treatment as compared with saline. In addition, the cytokines related to NF-κB pathway were also measured by ELISA (Fig. 6H–L), where the pro-inflammatory cytokines, such as TNF-α, IL-1β, IL-6, COX-2 and iNOS, were distinctly suppressed by the LAID treatment rather than saline. Hence, LAID could perform a lipid-inflammation integrated regulation on foam cells through lipid uptake inhibition and NF-κB pathway blockage, which synergistically restrained the NF-κB mediated inflammation.

The mechanism of lipid-inflammation integrated regulation was further studied on atherosclerotic mice with LAIP or LAID treatment following the protocol in Fig. 4A. As shown in Fig. 6M, the sections of aortic roots were used to stained with antibodies to NF-κB, CD36 and Sortilin. It could be discovered that both LAIP and LAID demonstrated a significant limitation on NF-κB, CD36 and Sortilin expression, while LAID showed a better inhibition than LAIP on account of its better accumulation provided by the active targeting ability (Fig. 6N–P). On the other side, the typical cytokines of TNF-α, IL-1β, IL-6, COX-2 and iNOS expressed in aortic tissue were also calculated and shown in Fig. 6Q–U. In keeping with the *in vitro* result, LAIP and LAID showed an inhibited inflammatory reaction stimulated by NF-κB pathway, while LAID could offer a better anti-inflammation effect than LAIP. Therefore, the lipid-inflammation integrated regulation of LAID on atherosclerosis progression was performed through inhibiting CD36 and Sortilin for lipid uptake limitation, and suppressing NF-κB pathway for anti-inflammation, where the restrained CD36 and Sortilin also assisted the blockage of NF-κB pathway.

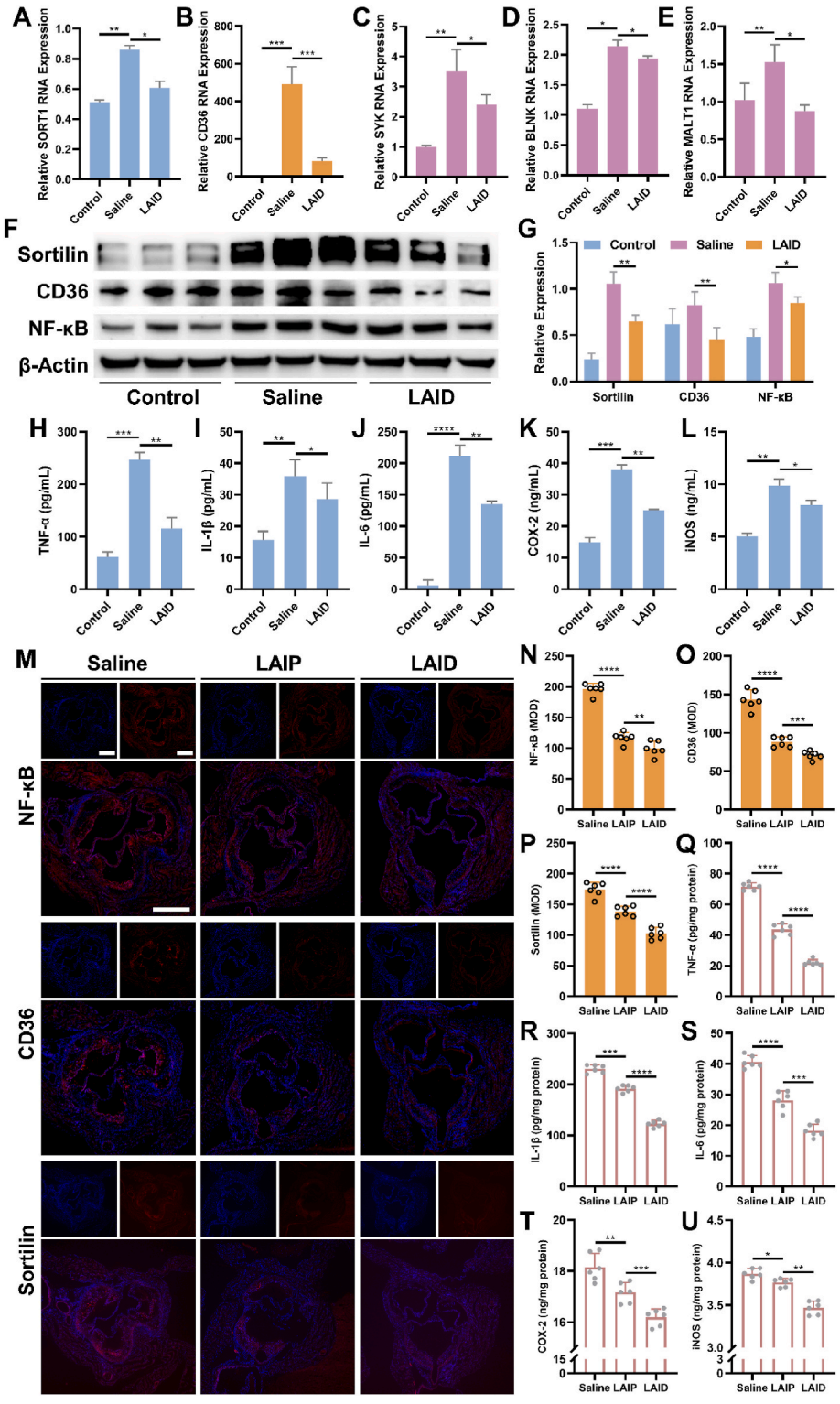

Fig. 6. Mechanism studies of LAID on foam cells and atherosclerotic lesions. Quantitative results of real-time PCR on RNA of A) Sort1, B) Cd36, C) Syk, D) Blnk and E) Malt1 extracted from foam cells with various treatment. F) Western blot bands and G) quantified data of CD36, Sortilin and NF-κB proteins on foam cells after different stimulations. Inflammatory cytokines of H) TNF-α, I) IL-1β, J) IL-6, K) COX-2 and L) iNOS were measured from foam cells. M) Photograph and quantitative result of aortic sections stained with fluorescently-labeled antibodies to N) NF-κB, O) CD36 and P) Sortilin after different treatments. The scale bars were 200 μm. Inflammation related cytokines such as Q) TNF-α, R) IL-1β, S) IL-6, T) COX-2 and U) iNOS expressed in aortic tissues. Data in (A-E, G-L, N–U) are expressed as mean ± s.d. (A-E, G-L, n = 3; N–U, n = 6). $^{*}p < 0.05$, $^{**}p < 0.01$, $^{***}p < 0.001$, $^{****}p < 0.0001$.

3. Conclusion

In conclusion, aiming at the theranostics of early-stage vulnerable plaque, we described a LAID nanoplatform with dual-mode diagnosis and lipid-inflammation integrated treatment. LAID was constructed with astaxanthin as the therapeutic module, ICA as the plaque-recognition module and oxDEX as the active targeting module, while the lipid-specific probe LFP was loaded into the cores. The active targeting ability of LAID promised an efficient accumulation at atherosclerotic lesions, while its dual-responsiveness to local overexpressed ROS and acidic environment indicated the timely disassembly of nanoplatform for further precise theranostics. The ICA revealed a distinct signal under X-CT, which located the early-stage plaques without blood-limiting symptoms. In further, LFP offered a favorable lipid-specific fluorescent imaging of the lipid cores in vulnerable plaques, resulting in the accurate recognition of the unstable plaque with higher prognostic risk. At the same time, the lipid-inflammation integrated regulation on the lesions was performed by LAID, which led to the effective restrain to the progression of atherosclerosis. The mechanism study of treatment based on RNA-sequencing analysis demonstrated that five typical genes (Cd36, Sort1, Syk, Blnk and Malt1) were suppressed, which contributed to the inhibition of CD36 and Sortilin protein for reduced lipid uptake and the blockage of BCR-PKC–NF–κB pathway for anti-inflammation. Besides, the reduced CD36 and Sortilin also synergistically assisted the down-regulation of NF-κB pathway. In together, LAID realized a precise diagnosis on early-stage vulnerable plaques and accomplished a lipid-inflammation integrated regulation on atherosclerotic lesions, which provided a novel perspective for clinical theranostics of atherosclerosis in early stage.

4. Experimental section

4.1. Preparation of LAID nanoparticles

AST (9 mg) and ICA (14 mg) were dissolved in 10 mL DMSO with the addition of LFP (20 mg). After stirred for 24 h, oxDEX (40 mg) dissolved in 1 mL PBS were added into the solution and stirred for another 12 h. Afterwards, the solution was dropwise added into 10 mL of PBS, which was further dialyzed against PBS after 2 h of stirring. The LAID solution was obtained after 24 h of dialysis and extrusion through the 0.22 μm syringe filter. The drug loading content of AST was calculated as 15.4%, while the drug loading efficiency was 73.7%. The loading content of LFP was determined to be 14.4% with a loading efficiency of 52.5%. On the other hand, the molar ratio of ICA grafted on oxDEX was calculated to be 5:8. Following the similar procedure, LAIP nanoparticles were also prepared by replacing the oxDEX with the equal weight of PEG-CHO.

4.2. In vivo dual-mode imaging of atherosclerosis plaques

LAID (10 mg kg^{-1}) and saline as the control were injected intravenously into the $ApoE^{-/-}$ mice after 8 weeks of high-fat diet. After 12 h from the injection, the Milabs X-CT system was used to detect the signals of nanoparticles in order to locate the plaques. Furthermore, the aortas were isolated from the mice and the fluorescent signals on *en* face and sections of the plaques were observed using CLSM. The lipid specific green fluorescence was identified as the lipid core of the plaques. To confirm the accuracy of diagnosis, the aortic tissue with lipid-specific fluorescent signals were prepared as the sections, which were further stained with ORO, H&E and Masson.

4.3. In vivo treatment against atherosclerosis

$ApoE^{-/-}$ mice were fed with high-fat diet (HFD) for 8 weeks to construct the atherosclerotic lesions, which were divided randomly into 6 groups. The solutions of saline, LAIP or LAID (10 mg kg^{-1}) were intravenously injected every two days for another 4 weeks fed with HFD. At the end of treatment, the mice were sacrificed. The aortas were separated and stained with ORO while the sections of the aortic arch were also prepared. ORO, H&E and Masson were used to perform the sections staining as well as the immunohistochemistry studies such as antibodies to α-smooth muscle actin (α-SMA), CD68, and matrix metalloproteinase-9 (MMP-9). The ratio of stain-positive area to the vascular lumen area was calculated.

To evaluate the lipid-inflammation integrated regulation on atherosclerotic lesions, the immunofluorescence sections were prepared using antibodies to NF-κB, CD36 and Sortilin. What's more, the tissue homogenate of aortas was prepared where typical inflammatory cytokines (TNF-α, IL-1β, IL-6, COX-2 and iNOS) were measured using ELISA.

4.4. RNA sequencing analysis

The foam cells were cultured for 48 h with treatment of saline and LAID. Then the cells were collected and the total RNA was extracted using TRIzol reagent (MajorBio Technology). The gene expression in RNA-seq was measured with transcript per million (TPM). The differentially expressed genes (DEGs) were identified using edgeR package with adjusted p-value <0.01 and $|\log2FC| > 0.87$.

Ethics approval and consent to participate

All animal experiments were approved by the Laboratory Animal Research Center of Sir Run Run Shaw Hospital, Zhejiang University School of Medicine. The animal protocols were assessed and approved by the Animal Laboratory Ethics Committee of Zhejiang University (SYXK2017-0006).

Declaration of competing interestCOI

The authors declare that they have no known competing financial interests or personal relationships that could have appeared to influence the work reported in this paper.

CRediT authorship contribution statement

Yao Wang: Software, Methodology, Data curation. **Zhebin Chen:** Investigation, Formal analysis, Data curation. **Qiongjun Zhu:** Software, Resources, Methodology. **Zhezhe Chen:** Software, Resources. **Guosheng Fu:** Supervision, Funding acquisition, Conceptualization. **Boxuan Ma:** Writing – review & editing, Supervision, Project administration, Funding acquisition, Formal analysis, Conceptualization. **Wenbin Zhang:** Writing – review & editing, Supervision, Resources, Project administration, Funding acquisition.

Acknowledgements

This research was financially supported by National Natural Science Foundation of China (No. 32201128, No. 82270262, and No. 82070408), Zhejiang TCM Science and Technology Program TCM modernization Special project, China (No. 2022ZX012). The schematic figures were created BioRender.com.

Appendix A. Supplementary data

Supplementary data to this article can be found online at https://doi.org/10.1016/j.bioactmat.2024.03.019.

References

[1] J. Shu, G. Santulli, Update on peripheral artery disease: epidemiology and evidence-based facts, Atherosclerosis 275 (2018) 379–381.
[2] P. Libby, J.E. Buring, L. Badimon, G.K. Hansson, J. Deanfield, M.S. Bittencourt, L. Tokgözoğlu, E.F. Lewis, Atherosclerosis, Nat. Rev. Dis. Prim. 5 (1) (2019) 56.

[3] S.M. Nidorf, A.T.L. Fiolet, A. Mosterd, J.W. Eikelboom, A. Schut, T.S.J. Opstal, S.H. K. The, X.F. Xu, M.A. Ireland, T. Lenderink, D. Latchem, P. Hoogslag, A. Jerzewski, P. Nierop, A. Whelan, R. Hendriks, H. Swart, J. Schaap, A.F.M. Kuijper, M.W.J. van Hessen, P. Saklani, I. Tan, A.G. Thompson, A. Morton, C. Judkins, W.A. Bax, M. Dirksen, M. Alings, G.J. Hankey, C.A. Budgeon, J.G.P. Tijssen, J.H. Cornel, P. L. Thompson, I. LoDoCo2 trial, colchicine in patients with chronic coronary disease, N. Engl. J. Med. 383 (19) (2020) 1838–1847.

[4] G.W. van Lammeren, H.M. den Ruijter, J.E.P. Vrijenhoek, S.W. van der Laan, E. Velema, J.-P.P.M. de Vries, D.P.V. de Kleijn, A. Vink, G.J. de Borst, F.L. Moll, M. L. Bots, G. Pasterkamp, Time-dependent changes in atherosclerotic plaque composition in patients undergoing carotid surgery, Circulation 129 (22) (2014) 2269–+.

[5] P. Libby, The changing landscape of atherosclerosis, Nature 592 (7855) (2021) 524–533.

[6] G.L. Basatemur, H.F. Jorgensen, M.C.H. Clarke, M.R. Bennett, Z. Mallat, Vascular smooth muscle cells in atherosclerosis, Nat. Rev. Cardiol. 16 (12) (2019) 727–744.

[7] C. He, S.C. Medley, T. Hu, M.E. Hinsdale, F. Lupu, R. Virmani, L.E. Olson, PDGFRbeta signalling regulates local inflammation and synergizes with hypercholesterolaemia to promote atherosclerosis, Nat. Commun. 6 (2015) 7770.

[8] J. Hitzel, E. Lee, Y. Zhang, S.I. Bibli, X. Li, S. Zukunft, B. Pfluger, J. Hu, C. Schurmann, A.E. Vasconez, J.A. Oo, A. Kratzer, S. Kumar, F. Rezende, I. Josipovic, D. Thomas, H. Giral, Y. Schreiber, G. Geisslinger, C. Fork, X. Yang, F. Sigala, C.E. Romanoski, J. Kroll, H. Jo, U. Landmesser, A.J. Lusis, D. Namgaladze, I. Fleming, M.S. Leisegang, J. Zhu, R.P. Brandes, Oxidized phospholipids regulate amino acid metabolism through MTHFD2 to facilitate nucleotide release in endothelial cells, Nat. Commun. 9 (1) (2018) 2292.

[9] J.M. Tarkin, M.R. Dweck, N.R. Evans, R.A. Takx, A.J. Brown, A. Tawakol, Z. A. Fayad, J.H. Rudd, Imaging atherosclerosis, Circ. Res. 118 (4) (2016) 750–769.

[10] M.M. Chowdhury, A. Tawakol, F.A. Jaffer, Molecular imaging of atherosclerosis: a clinical focus, Curr Cardiovasc Imaging Rep 10 (1) (2017).

[11] A.J. Beer, J. Pelisek, P. Heider, A. Saraste, C. Reeps, S. Metz, S. Seidl, H. Kessler, H.-J. Wester, H.H. Eckstein, M. Schwaiger, PET/CT imaging of integrin alpha v beta 3 expression in human carotid atherosclerosis, Jacc-Cardiovascular Imaging 7 (2) (2014) 178–187.

[12] C.Z. Behm, B.A. Kaufmann, C. Carr, M. Lankford, J.M. Sanders, C.E. Rose, S. Kaul, J.R. Lindner, Molecular imaging of endothelial vascular cell adhesion molecule-1 expression and inflammatory cell recruitment during vasculogenesis and ischemia-mediated arteriogenesis, Circulation 117 (22) (2008) 2902–2911.

[13] M.C. Press, F.A. Jaffer, Molecular intravascular imaging approaches for atherosclerosis, Curr Cardiovasc Imaging Rep 7 (10) (2014) 9293.

[14] N. Bettencourt, A. Chiribiri, A. Schuster, N. Ferreira, F. Sampaio, G. Pires-Morais, L. Santos, B. Melica, A. Rodrigues, P. Braga, L. Azevedo, M. Teixeira, A. Leite-Moreira, J. Silva-Cardoso, E. Nagel, V. Gama, Direct comparison of cardiac magnetic resonance and multidetector computed tomography stress-rest perfusion imaging for detection of coronary artery disease, J. Am. Coll. Cardiol. 61 (10) (2013) 1099–1107.

[15] S. Achenbach, K. Boehmer, T. Pflederer, D. Ropers, M. Seltmann, M. Lell, K. Anders, A. Kuettner, M. Uder, W.G. Daniel, M. Marwan, Influence of slice thickness and reconstruction kernel on the computed tomographic attenuation of coronary atherosclerotic plaque, J. Cardiovasc. Comput. Tomogr. 4 (2) (2010) 110–115.

[16] F. Caobelli, F.M. Bengel, In vivo evaluation of atherosclerotic plaques and culprit lesions using noninvasive techniques, Nat. Rev. Cardiol. 12 (2) (2015) 79. U31.

[17] P. Maffia, B.H. Zinselmeyer, A. Ialenti, S. Kennedy, A.H. Baker, I.B. McInnes, J. M. Brewer, P. Garside, Images in cardiovascular medicine. Multiphoton microscopy for 3-dimensional imaging of lymphocyte recruitment into apolipoprotein-E-deficient mouse carotid artery, Circulation 115 (11) (2007) e326–e328.

[18] A. Broisat, J. Toczek, L.S. Dumas, M. Ahmadi, S. Bacot, P. Perret, L. Slimani, G. Barone-Rochette, A. Soubies, N. Devoogdt, T. Lahoutte, D. Fagret, L.M. Riou, C. Ghezzi, Tc-99m-cAbVCAM1-5 imaging is a sensitive and reproducible tool for the detection of inflamed atherosclerotic lesions in mice, J. Nucl. Med. 55 (10) (2014) 1678–1684.

[19] K. Musunuru, S. Kathiresan, Surprises from genetic analyses of lipid risk factors for atherosclerosis, Circ. Res. 118 (4) (2016) 579–585.

[20] A. Mehlem, C.E. Hagberg, L. Muhl, U. Eriksson, A. Falkevall, Imaging of neutral lipids by oil red O for analyzing the metabolic status in health and disease, Nat. Protoc. 8 (6) (2013) 1149–1154.

[21] E. Kim, S. Lee, S.B. Park, A Seoul-Fluor-based bioprobe for lipid droplets and its application in image-based high throughput screening, Chem. Commun. 48 (17) (2012) 2331–2333.

[22] K.W. Howell, X. Meng, D.A. Fullerton, C. Jin, T.B. Reece, J.C. Cleveland Jr., Toll-like receptor 4 mediates oxidized LDL-induced macrophage differentiation to foam cells, J. Surg. Res. 171 (1) (2011) e27–e31.

[23] D.R. Lewis, L.K. Petersen, A.W. York, S. Ahuja, H. Chae, L.B. Joseph, S. Rahimi, K. E. Uhrich, P.B. Haser, P.V. Moghe, Nanotherapeutics for inhibition of atherogenesis and modulation of inflammation in atherosclerotic plaques, Cardiovasc. Res. 109 (2) (2015) 283–293.

[24] K. Cui, X. Gao, B. Wang, H. Wu, K. Arulsamy, Y. Dong, Y. Xiao, X. Jiang, M. V. Malovichko, K. Li, Q. Peng, Y.W. Lu, B. Zhu, R. Zheng, S. Wong, D.B. Cowan, M. Linton, S. Srivastava, J. Shi, K. Chen, H. Chen, Epsin nanotherapy regulates cholesterol transport to fortify atheroma regression, Circ. Res. 132 (1) (2023) e22–e42.

[25] A.H. Ali, N. Younis, R. Abdallah, F. Shaer, A. Dakroub, M.A. Ayoub, R. Iratni, H. M. Yassine, K. Zibara, A. Orekhov, A.F. El-Yazbi, A.H. Eid, Lipid-lowering therapies for atherosclerosis: statins, fibrates, ezetimibe and PCSK9 monoclonal antibodies, Curr. Med. Chem. 28 (36) (2021) 7427–7445.

[26] R.P. Giugliano, T.R. Pedersen, J.-G. Park, G.M. De Ferrari, Z.A. Gaciong, R. Ceska, K. Toth, I. Gouni-Berthold, J. Lopez-Miranda, F. Schiele, F. Mach, B.R. Ott, E. Kanevsky, A.L. Pineda, R. Somaratne, S.M. Wasserman, A.C. Keech, P.S. Sever, M.S. Sabatine, F. Investigators, Clinical efficacy and safety of achieving very low LDL-cholesterol concentrations with the PCSK9 inhibitor evolocumab: a prespecified secondary analysis of the FOURIER trial, Lancet 390 (10106) (2017) 1962–1971.

[27] K.M. Hallow, W.R. Taylor, A. Rachev, R.P. Vito, Markers of inflammation collocate with increased wall stress in human coronary arterial plaque, Biomech. Model. Mechanobiol. 8 (6) (2009) 473–486.

[28] M. Back, A. Yurdagul Jr., I. Tabas, K. Oorni, P.T. Kovanen, Inflammation and its resolution in atherosclerosis: mediators and therapeutic opportunities, Nat. Rev. Cardiol. 16 (7) (2019) 389–406.

[29] R. Khan, V. Spagnoli, J.-C. Tardif, P.L. L'Allier, Novel anti-inflammatory therapies for the treatment of atherosclerosis, Atherosclerosis 240 (2) (2015) 497–509.

[30] P.M. Ridker, B.M. Everett, T. Thuren, J.G. MacFadyen, W.H. Chang, C. Ballantyne, F. Fonseca, J. Nicolau, W. Koenig, S.D. Anker, J.J.P. Kastelein, J.H. Cornel, P. Pais, D. Pella, J. Genest, R. Cifkova, A. Lorenzatti, T. Forster, Z. Kobalava, L. Vida-Simiti, M. Flather, H. Shimokawa, H. Ogawa, M. Dellborg, P.R.F. Rossi, R.P.T. Troquay, P. Libby, R.J. Glynn, C.T. Grp, Antiinflammatory therapy with canakinumab for atherosclerotic disease, N. Engl. J. Med. 377 (12) (2017) 1119–1131.

[31] M.E. Lobatto, V. Fuster, Z.A. Fayad, W.J. Mulder, Perspectives and opportunities for nanomedicine in the management of atherosclerosis, Nat. Rev. Drug Discov. 10 (11) (2011) 835–852.

[32] T. Dvir, B.P. Timko, D.S. Kohane, R. Langer, Nanotechnological strategies for engineering complex tissues, Nat. Nanotechnol. 6 (1) (2011) 13–22.

[33] H.S. Choi, J.V. Frangioni, Nanoparticles for biomedical imaging: fundamentals of clinical translation, Mol. Imag. 9 (6) (2010) 291–310.

[34] T.M. Allen, P.R. Cullis, Drug delivery systems: entering the mainstream, Science 303 (5665) (2004) 1818–1822.

[35] M. Liu, H. Lutz, D. Zhu, K. Huang, Z. Li, P.-U.C. Dinh, J. Gao, Y. Zhang, K. Cheng, Bispecific antibody inhalation therapy for redirecting stem cells from the lungs to repair heart injury, Adv. Sci. 8 (1) (2021) 2002127.

[36] Z. Li, S. Hu, K. Huang, T. Su, J. Cores, K. Cheng, Targeted anti–IL-1β platelet microparticles for cardiac detoxing and repair, Sci. Adv. 6 (6) (2020) eaay0589.

[37] F.A. Jaffer, P. Libby, R. Weissleder, Optical and multimodality molecular imaging: insights into atherosclerosis, Arterioscler. Thromb. Vasc. Biol. 29 (7) (2009) 1017–1024.

[38] H.N. Hodis, J.K. Amartey, D.W. Crawford, E. Wickham, R.C. Sharma, D. H. Blankenhorn, Relationship of arterial-wall uptake of radiolabeled liposomes to the presence of monocyte macrophage cells in the hypertensive and atherosclerotic arterial-wall, Atherosclerosis 87 (2–3) (1991) 109–117.

[39] J. Kim, L. Cao, D. Shvartsman, E.A. Silva, D.J. Mooney, Targeted delivery of nanoparticles to ischemic muscle for imaging and therapeutic angiogenesis, Nano Lett. 11 (2) (2011) 694–700.

[40] M. Joner, K. Morimoto, H. Kasukawa, K. Steigerwald, S. Merl, G. Nakazawa, M. C. John, A.V. Finn, E. Acampado, F.D. Kolodgie, H.K. Gold, R. Virmani, Site-specific targeting of nanoparticle prednisolone reduces in-stent restenosis in a rabbit model of established atheroma, Arterioscler. Thromb. Vasc. Biol. 28 (11) (2008) 1960. U113.

[41] D.B. Kirpotin, D.C. Drummond, Y. Shao, M.R. Shalaby, K. Hong, U.B. Nielsen, J. D. Marks, C.C. Benz, J.W. Park, Antibody targeting of long-circulating lipidic nanoparticles does not increase tumor localization but does increase internalization in animal models, Cancer Res. 66 (13) (2006) 6732–6740.

[42] P. Libby, J. Loscalzo, P.M. Ridker, M.E. Farkouh, P.Y. Hsue, V. Fuster, A.A. Hasan, S. Amar, Inflammation, immunity, and infection in atherothrombosis JACC review topic of the week, J. Am. Coll. Cardiol. 72 (17) (2018) 2071–2081.

[43] E. Falk, Pathogenesis of atherosclerosis, J. Am. Coll. Cardiol. 47 (8) (2006) C7–C12.

[44] L. Montero de Espinosa, W. Meesorn, D. Moatsou, C. Weder, Bioinspired polymer systems with stimuli-responsive mechanical properties, Chem. Rev. 117 (20) (2017) 12851–12892.

[45] Y. Liu, C.F. Xu, S. Iqbal, X.Z. Yang, J. Wang, Responsive nanocarriers as an emerging platform for cascaded delivery of nucleic acids to cancer, Adv. Drug Deliv. Rev. 115 (2017) 98–114.

[46] H. Xu, P. She, Z. Zhao, B. Ma, G. Li, Y. Wang, Duplex responsive nanoplatform with cascade targeting for atherosclerosis photoacoustic diagnosis and multichannel combination therapy, Adv. Mater. (2023) e2300439.

[47] X. Hou, H. Lin, X. Zhou, Z. Cheng, Y. Li, X. Liu, F. Zhao, Y. Zhu, P. Zhang, D. Chen, Novel dual ROS-sensitive and CD44 receptor targeting nanomicelles based on oligomeric hyaluronic acid for the efficient therapy of atherosclerosis, Carbohydrate Polym. 232 (2020).

[48] M. Liu, A.R. Khan, J. Ji, G. Lin, X. Zhao, G. Zhai, Crosslinked self-assembled nanoparticles for chemo-sonodynamic combination therapy favoring antitumor, antimetastasis management and immune responses, J. Contr. Release 290 (2018) 150–164.

[49] M. Liu, H. Du, A.R. Khan, J. Ji, A. Yu, G. Zhai, Redox/enzyme sensitive chondroitin sulfate-based self-assembled nanoparticles loading docetaxel for the inhibition of metastasis and growth of melanoma, Carbohydrate Polym. 184 (2018) 82–93.

[50] M. Liu, H. Du, W. Zhang, G. Zhai, Internal stimuli-responsive nanocarriers for drug delivery: design strategies and applications, Mater. Sci. Eng. C 71 (2017) 1267–1280.

[51] M. Liu, H. Du, G. Zhai, Self-assembled nanoparticles based on chondroitin sulfate-deoxycholic acid conjugates for docetaxel delivery: effect of degree of substitution of deoxycholic acid, Colloids Surf. B Biointerfaces 146 (2016) 235–244.
[52] X. Liu, J. Xie, L. Zhou, J. Zhang, Z. Chen, J. Xiao, Y. Cao, H. Xiao, Recent advances in health benefits and bioavailability of dietary astaxanthin and its isomers, Food Chem. 404 (Pt B) (2023) 134605.
[53] Z. Zhu, J. Li, R. Tong, X. Zhang, B. Yu, Astaxanthin suppresses End MT by LOX-1 pathway in ox-LDL-induced HUVECs, Eur. J. Inflamm. 20 (2022).
[54] T.B. Zou, S.S. Zhu, F. Luo, W.Q. Li, X.R. Sun, H.F. Wu, Effects of astaxanthin on reverse cholesterol transport and atherosclerosis in mice, BioMed Res. Int. 2017 (2017) 4625932.
[55] Y. Kishimoto, M. Tani, H. Uto-Kondo, M. Iizuka, E. Saita, H. Sone, H. Kurata, K. Kondo, Astaxanthin suppresses scavenger receptor expression and matrix metalloproteinase activity in macrophages, Eur. J. Nutr. 49 (2) (2010) 119–126.
[56] C. Li, Y. Dou, Y. Chen, Y. Qi, L. Li, S. Han, T. Jin, J. Guo, J. Chen, J. Zhang, Site-specific MicroRNA-33 antagonism by pH-responsive nanotherapies for treatment of atherosclerosis via regulating cholesterol efflux and adaptive immunity, Adv. Funct. Mater. 30 (42) (2020) 2002131.
[57] Q. Yang, H. Jiang, Y. Wang, X. Leng, Y. Wang, J. Tong, Y. Zhou, C. Mo, J. Peng, H. Gao, Plaque macrophage-targeting nanosystems with cooperative Co-regulation of ROS and TRAF6 for stabilization of atherosclerotic plaques, Adv. Funct. Mater. 33 (28) (2023) 2301053.
[58] H. Yaghooti, N. Mohammadtaghvaei, K. Mahboobnia, Effects of palmitate and astaxanthin on cell viability and proinflammatory characteristics of mesenchymal stem cells, Int. Immunopharm. 68 (2019) 164–170.
[59] C.-S. Lin, F.-Y. Lin, L.-J. Ho, C.-S. Tsai, S.-M. Cheng, W.-L. Wu, C.-Y. Huang, C.-H. Lian, S.-P. Yang, J.-H. Lai, PKCδ signalling regulates SR-A and CD36 expression and foam cell formation, Cardiovasc. Res. 95 (3) (2012) 346–355.
[60] A.C. Nicholson, M. Febbraio, J. Han, R.L. Silverstein, D.P. Hajjar, CD36 in atherosclerosis: the role of a class B macrophage scavenger receptor, Ann. N. Y. Acad. Sci. 902 (1) (2000) 128–133.
[61] D.J. Van Antwerp, S.J. Martin, I.M. Verma, D.R. Green, Inhibition of TNF-induced apoptosis by NF-kB, Trends Cell Biol. 8 (3) (1998) 107–111.
[62] A.A. Beg, D. Baltimore, An essential role for NF-κB in preventing TNF-α-Induced cell death, Science 274 (5288) (1996) 782–784.